Electronic materials

CrossMark

Evolution of glassy carbon under heat treatment: correlation structure–mechanical properties

K. Jurkiewicz[1,2,*] , M. Pawlyta[3] , D. Zygadło[1,2] , D. Chrobak[2,4] , S. Duber[5] ,
R. Wrzalik[1,2] , A. Ratuszna[1,2] , and A. Burian[1,2]

[1] *A. Chełkowski Institute of Physics, University of Silesia, ul. Uniwersytecka 4, 40-007 Katowice, Poland*

[2] *Silesian Center for Education and Interdisciplinary Research, ul. 75 Pułku Piechoty 1A, 41-500 Chorzow, Poland*

[3] *Institute of Engineering Materials and Biomaterials, Silesian University of Technology, ul. Konarskiego 18A, 44-100 Gliwice, Poland*

[4] *Institute of Materials Science, University of Silesia, ul. 75 Pułku Piechoty 1A, 41-500 Chorzow, Poland*

[5] *Laboratory of Structural Research, University of Silesia, 41-500 Chorzow, Poland*

ABSTRACT

In order to accommodate an increasing demand for glassy carbon products with tailored characteristics, one has to understand the origin of their structure-related properties. In this work, through the use of high-resolution transmission electron microscopy, Raman spectroscopy, and electron energy loss spectroscopy it has been demonstrated that the structure of glassy carbon at different stages of the carbonization process resembles the curvature observed in fragments of nanotubes, fullerenes, or nanoonions. The measured nanoindentation hardness and reduced Young's modulus change as a function of the pyrolysis temperature from the range of 600–2500 °C and reach maximum values for carbon pyrolyzed at around 1000 °C. Essentially, the highest values of the mechanical parameters for glassy carbon manufactured at that temperature can be related to the greatest amount of non-planar sp^2-hybridized carbon atoms involved in the formation of curved graphene-like layers. Such complex labyrinth-like structure with sp^2-type bonding would be rigid and hard to break that explains the glassy carbon high strength and hardness.

Introduction

The disordered, non-graphitizing glassy carbons, also called glass-like carbons, are typically synthesized by pyrolysis of polymeric precursor such as phenolic resins or polyfurfuryl alcohol [1–4]. Due to their relative ease of production and a diverse range of physical properties, such as high thermal resistance, extreme chemical stability, low density and great hardness compared with other carbons, gases impermeability, and high electrical conductivity, these carbons have been extensively industrially applied since decades. In addition, glassy carbons exhibit excellent biologic compatibility with blood and tissues, meaning that they have a high potential for use in medicine [5]. The most recent studies have

suggested that glassy carbons have a fullerene-related structure. Such model of the structure, proposed by Harris [2, 6–8], consists of broken and imperfect fullerene fragments in the form of curved sp^2-bonded graphene-like planes, which can be multilayered and which often surround closed pores. The presence of curvature has been attributed to the topological defects in the form of non-hexagonal carbon rings such as pentagons and heptagons that were directly observed by the high-resolution transmission electron microscope (HRTEM) [9]. When glassy carbons are exposed to the temperature, the building structural blocks start ordering within individual graphene-like layers and the number of layers increases [2, 6–8, 10, 11]. Ordering within the layers is accompanied by increase in their sizes. However, even after heat treatment at temperatures of 3000 °C and above the glassy carbons cannot be transformed into crystalline graphite [7, 10] and preserve the general type of atomic disorder remaining features of the paracrystalline structure [12].

The structure is a key factor determining glassy carbon porosity, mechanical, and electronic properties. Therefore, the possibility to control the temperature-induced structural transformation is critically important for the fabrication of the glassy carbon products with desired functional features. It is essential to note that novel glassy carbon applications, such as micro-electro-mechanical systems [13, 14], that can be used for medical prostheses [15, 16] require comprehensive characterization of the properties–structure relationships at both, bulk- and nanoscale level. But up to now, the knowledge on how the manufacturing temperature, that is, how the internal structure affects the properties of glassy carbons is insufficient. Herein, high-resolution transmission electron microscopy, Raman spectroscopy, electron energy loss spectroscopy (EELS), and nanoindentation measurements were performed on a series of glassy carbons prepared by pyrolysis of polyfurfuryl alcohol at different temperatures from the range 600–2500 °C to shed more light on the evolution of their structure and properties during the heat treatment. The main aim of this work is investigation of correlations between the structure of the glassy carbons changing under the thermal treatment and their mechanical characteristics.

Experimental details

Preparation of glassy carbons

The glassy carbons studied here were prepared from furfuryl alcohol as a precursor. Polymeric furfuryl alcohol-based samples were pyrolyzed under protective Ar gas flow. The heating rate was 10 °C/h to 200 °C and 5 °C/h to the different desired temperatures: 600, 800, and 980 °C. Upon reaching the final heat treatment level, the temperature was held constant for 2 h. Then, the carbonized samples were allowed to cool in Ar flow. Next, some of the samples carbonized at 980 °C were further heat treated at 1500, 2000, and 2500 °C in Ar atmosphere. The high-temperature processing was performed with the heating rate of 4 °C/min from the room temperature up to the maximum pyrolysis temperature with the samples residence time 2 h at the final temperature. The glassy carbons heat treated as described above at different temperatures ranging from 600 to 2500 °C are labeled here according to the maximum annealing temperature as GC600, GC800, GC980, GC1500, GC2000, and GC2500, respectively. The chemical composition of the prepared carbons was examined using the X-ray fluorescence spectroscopy. The C content, included in Table 1, increases monotonically and tends toward 100% for high-temperature carbonization. The presence of elements other than C and O was below 0.1 at.%. The densities of the samples were monitored using helium pycnometer and are presented in Table 1. The density is observed to be the highest at temperature of 800 °C. Above 800 °C, the density decreases significantly due to rearrangement of the structure, formation, and growth of closed pores and for GC2500 is around 1.51 g/cm^3. The observations of density changes with pyrolysis temperature are generally in agreement with behavior reported by Zhang et al. [17] for glassy carbons from phenolic resins.

High-resolution transmission electron microscopy and electron energy loss spectroscopy

TEM investigations were done on a probe Cs-corrected S/TEM Titan 80-300 FEI microscope, equipped with a Gatan Tridiem 863 spectrometer. The preparation of samples was performed as follows: The pyrolyzed glassy carbon disks were ground in a steel

Table 1 C content and helium density of the glass-like carbons pyrolyzed at different temperatures from the range 600–2500 °C

Glass-like carbon	C content $\pm$ 1 [%]	He density $\pm$ 0.01 [g/cm^3]
GC600	94	1.60
GC800	96	1.88
GC980	97	1.77
GC1500	98	1.55
GC2000	100	1.52
GC2500	100	1.51

mill, the obtained powders were dispersed in ethanol using an ultrasonic bath, and then droplets of such prepared dispersions were put onto a carbon—coated lacey substrate supported by a copper grid and dried at room temperature. HRTEM imaging was obtained at 300 kV. The images were recorded with 1 s exposure time to avoid radiation damage of samples.

EELS spectra were acquired at 80 kV in STEM mode. Lower acceleration voltage of the electron was applied to exclude the influence of the electron beam on the structure of the material under test [18, 19]. The measurements were performed in STEM mode, allowing for the proper selection of fragments for analysis—sufficiently thin and homogeneous. The fitting procedure of EELS bands was performed with the Fityk software [20].

Raman spectroscopy

The Raman spectra of the series of glassy carbons were obtained using WITec Alfa 300R Raman spectrometer equipped with a confocal microscope, a 532-nm Nd:YAG diode laser and a highly sensitive back-illuminated Newton-CCD camera. The data were collected at room temperature with a 50 × objective (NA = 0.5), accumulated with 10 s exposure time and 100 repetitions in the spectral range between 200 and 3500 cm^{-1}. For each glassy carbon sample, the Raman scattering was measured at different places to make sure that the probed materials are homogeneous and the collected spectra provide representative structural information of bulk material. The fitting procedure of Raman bands was performed with the Fityk software [20].

Nanoindentation

Nanoindentation tests were performed with the Hysitron TriboIndenter TI-950 system. We have used Berkovich diamond tip to conduct the mechanical tests. The maximum load applied to the indenter was

0.8 mN, while the load function was composed of three parts: 5 s loading, 2 s dwell time, and 5 s unloading. The thermal drift rate was less than 0.1 nm/s. All experiments were performed in a constant ambient temperature and humidity, shielding the equipment from external vibrations. The Berkovich tip was calibrated using the fused quartz as a standard. The key parameters obtained during the nanoindentation experiment were hardness (H) and reduced Young's modulus (E_r). They were estimated using the well-known Oliver–Pharr method [21] as follows:

$$H = \frac{P_{\max}}{A_r}, \tag{1}$$

where $P_{\max}$ is the maximum load and A_r is the residual indentation area;

$$\frac{1}{E_r} = \frac{1 - v^2}{E} + \frac{1 - v_{\text{ind}}^2}{E_{\text{ind}}}, \tag{2}$$

where E and v are the elastic modulus and Poisson's ratio of the sample, respectively, E_{ind} and v_{ind} are the same parameters of the diamond indenter tip.

Results

Comparative characterization of glassy carbon structural organization by HRTEM

The representative HRTEM images at different magnifications of the glassy carbons pyrolyzed at various temperatures, 600, 980, 1500, 2000, and 2500 °C are presented in Fig. 1. Black lines in these pictures represent parts of the carbon sheets which lie approximately parallel to the incident electron beam. The pictures show the evolution from a network of randomly oriented, disordered carbon domains to a more organized system resembling onion-like elements in which carbon layers are less rippled. The glassy carbon microstructure passes through a few
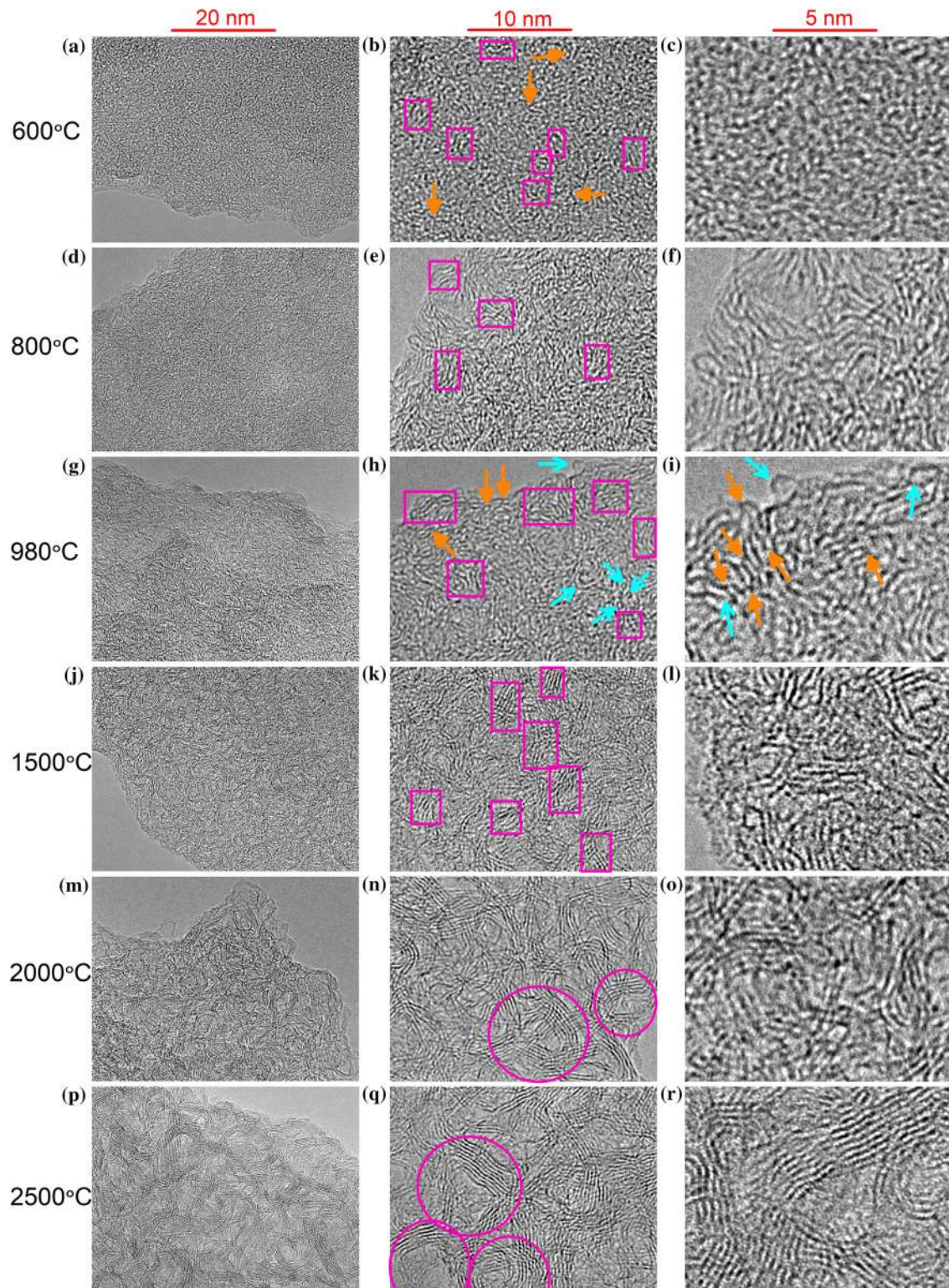
Figure 1 Representative HRTEM images at various magnifications of different regions of glassy carbon samples pyrolyzed at temperatures from the range 600–2500 °C. Rectangular frames expose domains with stacked graphene-like layers; round frames show onion-like structures enclosing pores; arrows indicate curved structural units.

phases during the conversion to its high-temperature form. The low-temperature glassy carbon (this pyrolyzed at 600 °C) is comprised of curled layers, as can be seen in Fig. 1a–c. Such curvature can arise from both, defects in the graphene-like domains and connections between them. The presence of bridges between the neighboring carbon domains is a natural consequence of the starting polymer network which undergoes extensive cross-linking [22] that was postulated by Franklin in early models of graphitizing and non-graphitizing carbons [10]. The microstructure of the GC600 sample is homogeneous. However, clusters of two, three, or even four layers of about 1–2 nm long that are arranged in stacks can be distinguished (marked in Fig. 1b by rectangular frames) in the overall tangle of randomly distributed carbon layers. Most of these carbon segments up to 1–2 nm long are bent. Completely flat layers are very rare. The distance between neighboring layers is irregular not only due to their curvature, but also cross-links and branches they create and which are marked in Fig. 1b with arrows. The gaps created between the curved layers may result in slit-shaped nanometer pores.

In the case of the GC800 and GC980 samples, in the HRTEM images (Fig. 1d–i) one can notice that some changes in the structure have been undergone due to the higher annealing temperature. Like the GC600, some of the layers are stacked in groups. In the case of the GC800 and GC980, however, the stacks are longer and there are definitely more packages of three, four, or even more layers which are aligned roughly parallel to each other (Fig. 1e, h). As regards the structural curvature, a few types of the curvature-related behavior can be distinguished. The first type refers to the corrugation of surface observed for almost every carbon layer in the structure. The expected source of such curvature is the presence of structural defects in the form of vacancies and non-hexagonal carbon rings causing the graphene-like sheet to transform from a planar to curved geometry [6, 23, 24]. The different types of defects may be created during the coalescence of structural units [25]. During pyrolysis, atoms are not in the thermodynamic equilibrium and many dangling bonds occur. The structure is allowed to eliminate them in the non-equilibrium conditions by the formation of polygons such as pentagons or heptagons or higher-membered rings resulting in the folding of carbon layers. It should be noted that the pentagon rings are

also originally present in the initial structure of the furfuryl alcohol polymer [22, 26] and they can partly survive at the later stages of heat treatment, as confirmed by Tondi et al. [27], causing out-of-plane ripples. In parallel, the curvature is created by the carbon layers which branch out or link together by forming the specific tubular caps, marked in Fig. 1h, i with filled arrows. Such type of bridges between adjacent carbon layers creates compact 3D network which may prevent graphitization and make the material strong.

With increasing the carbonization temperature above 800 °C, the curvature related with elements resembling fragments of fullerenes, onions or even completely closed fullerene-like particles is more prevalent. The different types of curved structural elements for the GC980 are marked with arrows in Fig. 1h, i.

On the further heat treatment up to 1500 °C, one can notice in Fig. 1j–l that within the microstructure of glassy carbon two parts mixing with each other can be clearly distinguished. The first part, more organized, consists of groups of stacked and more or less parallel planes, while the second part, globally disordered, is characterized by randomly oriented and twisted layers of various sizes. We observe that the glassy carbon crystallites grow at the expense of the more disordered part of the microstructure. The less-organized regions are consumed by the domains with parallel layers resulting in their growth, both in width and height, and simultaneously in creation of empty voids. In the low-temperature glassy carbons, the microporosity is a direct consequence of misalignment of the curved sheets or their packages. As the annealing temperature increases, the bigger pores are formed due to joining of disordered fragments to more ordered domains. This leads to the creation of isolated, non-connected voids such as these marked with circle frames in Fig. 1n, r. The HRTEM images pretty clearly exhibit that dimensions of the micropores are tunable by the heat treatment in the range of few angstroms to several nanometers. Up to the maximum annealing temperature 2500 °C, the gradual elongation of graphene-like layers, increase in their number in the stacks and growth of pores are observable. As the pyrolysis temperature increases, the onion-like carbon structures become more prevalent. The high-temperature GC2500 is mostly composed of well-organized great fragments of onions or even entire onions (Fig. 1p–r).

They are made up of the curved and faceted graphite-like crystallites up to around 10 nm long and 10 layers thick. The onion-like elements are interwoven together and limit pores which are much larger than in the low-temperature glass-like carbons.

Correlation of first- and second-order Raman peaks behavior with the structural transformation

The first-order Raman spectra display two main peaks between 1200 and 1700 cm^{-1}, as shown in Fig. 2a, which are characteristic features of graphitic carbons [28]. The peak at around 1600 cm^{-1} is called graphitic or simply G band and is due to optical phonon mode with E_{2g} symmetry associated with an in-plane stretching of sp^2-bonded carbon atoms. The peak at around 1350 cm^{-1} is called disorder-induced or D band and is not observed for single-crystal perfect graphite [29]. The origin of the D mode had long been debated, and more recently it was attributed to the double-resonant Raman scattering [30]. The spectra of the first-order Raman region normalized to the D band intensity and overlapped to better distinguish differences between them are presented in Fig. 2b. The main characteristic feature of these spectra is the increase in the D intensity (I_D) with respect to the G peak intensity (I_G) and sharpening of

the D peak width with increasing pyrolysis temperature up to 2500 °C. The ratio of intensities I_D/I_G or corresponding integrated areas upon D and G peaks is sometimes used to calculate the averaged in-plane size of graphitic domains (L_a). According to the formula proposed by Tuinstra and Koenig: $I_D/I_G \sim 1/L_a$ (the so-called T-K rule) [28]. In the case of the studied here glassy carbons by HRTEM images, we observe continuous growth of carbon layers with the heat treatment temperature. Therefore, the T-K rule does not appear to be fulfilled in this case. Ferrari and Robertson [31] showed that for amorphous and disordered carbons the development of the D peak indicates ordering, exactly opposite to the case of graphite. They argued that the T-K formula should not be valid at very small values of L_a, because for small L_a the D band strength is proportional to the probability of finding a sixfold aromatic ring in the carbon cluster that is proportional to the cluster area L_a^2. Therefore, they submitted a new dependence of the I_D to I_G ratio on the L_a size, namely $I_D/I_G \sim L_a^2$ for carbons containing small clusters with L_a below about 25 nm and suggested that such a behavior of Raman spectra would be possible for non-crystalline graphite progressively defected resulting in its amorphization. Experimental example of this behavior has been found, i.e., for glassy carbon implanted with ions, which exhibited decreasing I_D/I_G ratio

Figure 2 Overview of the Raman spectra for glassy carbons pyrolyzed at different temperatures from the range of 600–2500 °C (GC600–GC2500) (**a**); comparison of the normalized spectra for the first-order region (**b**) and the second-order region (**c**). The insets show the best fit of the experimental data for glassy carbon pyrolyzed at 1500 °C (GC1500).
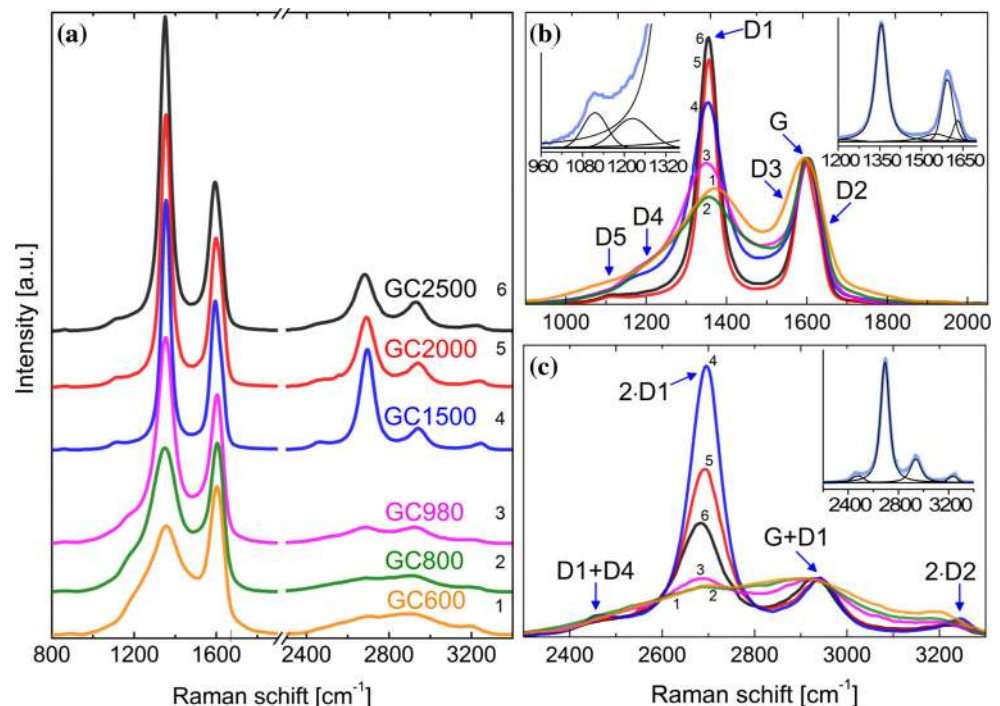
with higher ion doses due to loss in order and decrease in crystallite size [32]. Here, we observe a reverse process—the more disordered and fine carbon nucleuses are transformed during pyrolysis to less defected, better organized and greater packages of graphene layers and the I_D/I_G ratio increases with higher temperature. Similar tendency has been already observed for carbonized polyfurfuryl alcohol [33], cellulose [34], or wood [35].

In order to accurately recognize other bands contributing to Raman scattering for the glassy carbons, the spectra were fitted with the Voigt line shapes. A representative example of the fitting of the first- and second-order Raman spectra is showed for the glassy carbon heat treated at 1500 °C as insets in Fig. 2b, c. As a result of the fitting, we can distinguish six components contributing to the first-order Raman spectrum: (1) graphitic G peak at 1595 cm^{-1}, (2) disordered D1 peak at 1355 cm^{-1}, (3) D2 peak at 1630 cm^{-1} described in [29, 36], (4) D3 peak at 1549 cm^{-1} described in [28], (5) D4 peak at 1212 cm^{-1}, and (6) D5 peak at 1110 cm^{-1}. The D4 and D5 features must account for the total spectra during fitting of Raman data for all glassy carbon heat treated between 600 and 2500 °C; however, they weaken in intensity during the progressive heat treatment. Recently, Couzi et al. [37] showed that in the spectral range 1000–1300 cm^{-1} of various defective carbon materials three different components participate to the scattered signal and assigned them to the different defect-induced double resonance inter-valley processes. The idea of the defect-related history of the reported here D4 and D5 peaks seems to be reasonable. Interestingly, Fujimori et al. [38] experimentally identified a Raman signal from Stone–Thrower–Wales (STW) defects on single-walled carbon nanotubes in the range of 1100–1200 cm^{-1}. Moreover, according to theoretic calculations of the STW defect in a flat graphene two characteristic Raman modes at 1122 and 1173 cm^{-1} are predicted [39]. We assume that the D4 and D5 peaks observable here for the glassy carbons can also come from the vibrations of carbon atoms in non-hexagonal rings such as STW defects which are considered as the reason of the fullerene-like structure of glassy carbons [6–8].

The second-order Raman spectra compared in Fig. 2c reveal four peaks: (1) 2·D1 peak at 2695 cm^{-1}, (2) G + D1 peak at 2940 cm^{-1}, (3) 2·D2 at 3250 cm^{-1}, and (4) D1 + D4 at 2450 cm^{-1}. They are the overtones or the combined tones of the first-order bands.

For the low-temperature glassy carbons up to 1000 °C, the 2·D1 band merges with the other surrounding bands to form a small modulated bump. The intensity of the 2·D1 peak increases roughly six times for GC1500 in comparison with the GC980 and then decreases gradually for GC2000 and GC2500. It should be mentioned that the 2·D1 peak, named historically the G′ peak, for graphene is more intense than the G band compared to bulk graphite [39–42]. Increasing the number of graphene layers in the stack leads to a significant decrease in the 2·D1 to G intensity ratio [43, 44]. Indeed, for the glassy carbons we observe a systematic drop of the 2·D1 intensity with increase in the heat treatment temperature above the 1500 °C. That is probably the effect of increase in number of layers in the graphite-like domains, as can be seen in the electron microscopic images in Fig. 1. The lack of clearly pronounced peaks in the second-order region for the glassy carbons at 600, 800, and 980 °C may be due to a much lower intensity of the first-order Raman modes. Moreover, the low intensity of the 2·D1 bands for the low-temperature glassy carbons GC600–GC980 may be explained by the small lateral size of the graphene-like layers and/or very high defect densities causing strong distortion of graphene-like clusters. Further formation of greater and more uniform carbon hexagonal network for the GC1500 causes significant rise in the 2·D1 intensity.

Evidence of curved structural units in low-frequency Raman spectra

In the low-frequency region below 900 cm^{-1} of the measured spectra, a number of Raman-active modes were observed. All glassy carbons show peaks near 260 cm^{-1} (P1), 440 cm^{-1} (P2), 620 cm^{-1} (P3), and 860 cm^{-1} (P4), as can be seen in Fig. 3, while this Raman region is completely silent for graphite and diamond crystals according to the group theory [45]. Analogous bands in the low-frequency region of Raman spectra were found for carbon nanotubes, fullerenes, or nanoonions [46–50] as well for more exotic non-planar carbon structures such as tubular cones, whiskers, and polyhedral crystals [51]. Therefore, we assume that the observed modes are markers of curvature-related geometry in the investigated glassy carbons, which has been already confirmed by the HRTEM images.
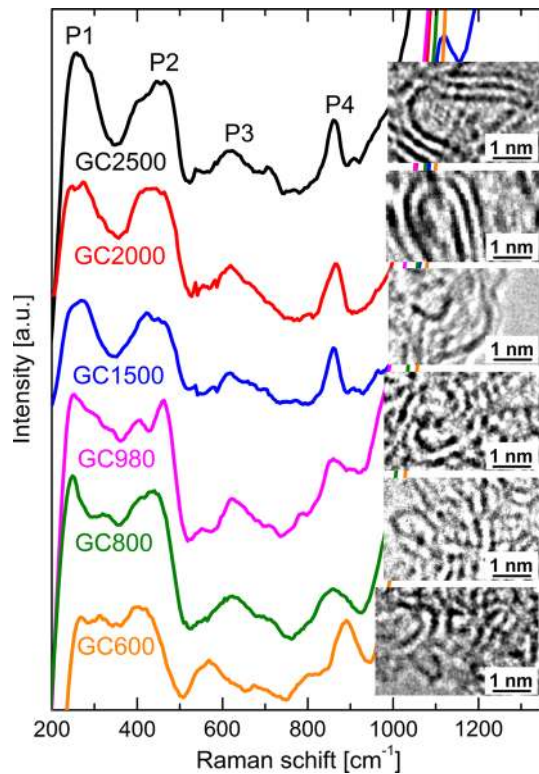
Figure 3 Low-frequency Raman modes for glassy carbons pyrolyzed up to different temperatures from the range of 600–2500 °C (GC600–GC2500). The insets show selected HRTEM images with curved structural units of around 1 nm in diameter.

It is known that a band in the range 100–350 cm^{-1} is a signature of single-walled carbon nanotubes (SWCNTs) and is related to their radial breathing modes (RBMs) unique to cylindrical symmetry [52]. The RBMs correspond to the coherent vibration of the carbon atoms where all the tube atoms vibrate radially in phase. Zhao et al. [53] established that the RBMs can also give active Raman peaks in the 100–600 cm^{-1} region for multi-walled carbon nanotubes (MWCNTs). These RBM frequencies (ω_{RBM}) are therefore very useful for identifying whether a given carbon material contains curved, nanotube-like elements. The ω_{RBM} depends on the nanotube diameter d as:

$$\omega_{RBM} = \frac{A}{d} + B, \tag{3}$$

where A and B are experimentally determined constants dependent on environment in which nanotube is present. The reported glassy carbon building blocks are multilayer nanostructures which can be classified as fragments of MWCNTs. It was

determined that for SWNTs of 1.5 nm in diameter measured in bundles $A = 234$ cm^{-1} and $B = 10$ cm^{-1} [53]. If we take the values of A and B parameters as mentioned above and we assume that recorded P1 peaks are 10% up-shifted due to interlayer interactions in multilayered domains [29], we are able to estimate the diameter of the nanotube fragments possibly responsible for the breathing vibrations to be of approximately 1 nm. Such nanotube-like elements of approximately 1 nm in diameter can be easily found in HRTEM images and their examples were attached as insets to Fig. 3.

Beside the P1 peak around 260 cm^{-1}, the Raman spectra contain also broad features with maxima at around 440 cm^{-1} (P2), 620 cm^{-1} (P3), and 860 cm^{-1} (P4). Herein reported low-frequency Raman modes for glassy carbons are analogs to the Raman features identified by Roy et al. [50] for carbon nanoonions produced by the arc discharge of graphite electrodes. Tan et al. [51] also observed Raman peaks at $\sim$ 470, 620, and 860 cm^{-1} in ion-implanted highly oriented pyrolytic carbon and in turbostratically stacked particles. Moreover, it was showed first time by Rao et al. [47] that SWCNTs exhibit numerous Raman modes in the region 300–1400 cm^{-1}. Two possible explanations for the origin of these peaks were proposed. One claims that these modes are combination of the acoustic and optical phonon modes activated due to nanotube geometry, and the other that they arise from structural defects [54]. Hence, it is clear that disorder and defects strongly influence the Raman spectra of carbon materials and the features reported here for glassy carbons in the range 350–900 cm^{-1} can be defect-induced Raman modes.

Bonding character of carbon atoms at different stages of thermal treatment

HRTEM and Raman spectroscopy results showed that glassy carbons at different stages of pyrolysis contain curved structural units. The question that arises is what type of bonds between carbon atoms the buckled layers contain. The presence of diamond-like sp^3-bonded atoms would explain the high hardness and resistance to graphitization of glassy carbons, and in the past an idea appeared that the sp^3-bonded carbons may act as potential cross-linking [55]. We used electron energy loss spectroscopy to estimate the amount of the possible sp^3 bonds as well

as to evaluate the sp^2-type bond character at different stages of the pyrolysis process.

The representative EELS spectra in the C-K edge region after background subtraction by fitting a power-low curve shown in Fig. 4a have two main features: the π* peak around 285 eV, caused by transitions from the carbon 1s core level to the anti-bonding state of π bonding, and the σ* peak around 291 eV, caused by transitions from the carbon 1s core level to the anti-bonding state of σ bonding. For GC600, the π* feature is broad and the σ* peak is poorly defined. With increase in pyrolysis temperature, the EELS spectra show an increase in the intensity of the π* peak in respect to the σ* peak intensity. Simultaneously, the σ* signal becomes more noticeable with rising temperature and the appearance of another weak features on the high energy side of the σ* peak, indicating an increase in longer range order [56]. Such a behavior of these spectra is typical for conversion of disorder carbon structure toward graphitic sp^2 bond configuration. However, the near-edge fine structure above 295 eV is less pronounced than in case for graphitic samples with three-dimensional crystalline order [56]. We used a procedure developed by Berger et al. [57] for determining the fraction of sp^2-bonded carbon atoms in the glassy carbons. This method is based on estimation of the ratio of integrated window centered upon the π* peak ($I_{\pi*}$) to the integrated area containing both, π* and σ* peaks ($I_{\pi*+\sigma*}$), according to the following equation:

$$\frac{sp^2}{sp^2 + sp^3} = \frac{I_{\pi*}}{I_{\pi*+\sigma*}} \quad (4)$$

Here, for calculations we used 6 eV window centered at 292 eV over the both π* and σ* peaks. The ratio obtained according to the (4) is usually normalized to the factor determined from spectra of a 100% sp^2-

hybridized material. The most often highly oriented pyrolytic graphite (HOPG) is used [56, 58]. However, an open discussion is correctness of such technique [59, 60]. Therefore, in order to avoid the uncertainty related with the choice of reference material we used the GC2500 sample as a reference in this series of glassy carbons. Based on recent studies by X-ray and neutron diffraction combined with molecular dynamic simulations [61] and the resulting optimized models of the glassy carbon atomic structures (available as .xyz files in the supporting information of the Ref. [61]), we determined the percentage amount of sp^3 carbon bonds in the proposed model of the GC2500 atomic structure to be about 0.5%. Therefore, we treat the glassy carbon heated at 2500 °C as a material containing near 100% sp^2 carbon hybridization. The computed changes in the sp^2-bonded C atoms content as a function of pyrolysis temperature with respect to the GC2500 reference are presented in Fig. 4b. The dispersion of the determined sp^2 fractions does not exceed 6% of the mean values. The fraction of sp^2 bonds is definitely over the fraction of sp^3 bonds, starting from about 95% for low-temperature glassy carbon GC600 and monotonically rising to almost 100% for GC2000. For low-temperature samples containing hydrogen, it is possible that we include intensity from electronic transition to the C–H(σ*) orbital giving signal about 287–289 eV, and the resulting content of sp^2 bonds determined by the procedure described above may be erroneously higher, as noticed by Daniels et al. [62].

Figure 5a shows example of a Gaussian fit to the C-K edge of glassy carbon pyrolyzed at 980 °C. Similar fits were employed for spectra of other glassy carbons. It is generally not possible to fit just one Gaussian peak to the 1s to π* transition range. An additional peak about 287 eV must be included even for high-temperature glassy carbons. It is unlikely that a significant amount of hydrogen can survive at

Figure 4 Variation in the glassy carbon electron energy loss in the C-K edge region (**a**), and in the determined sp^2-hybridized bond content (**b**) as a function of pyrolysis temperature from the range of 600–2500 °C (GC600–GC2500).
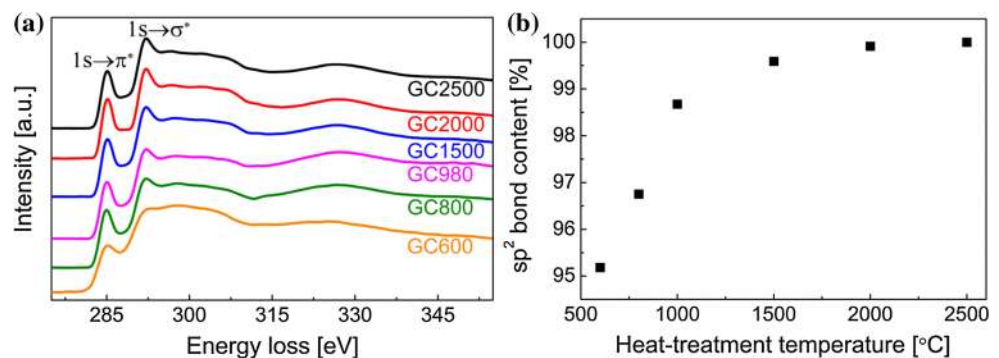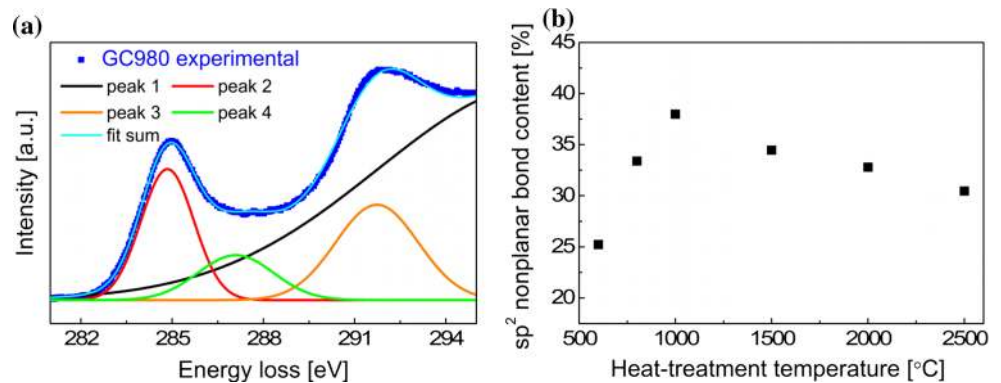
Figure 5 Example of a Gaussian fit to the C-K edge of glassy carbon pyrolyzed at 980 °C (GC980) (**a**), and variation in the sp^2-hybridized non-planar bond content as a function of pyrolysis temperature from the range of 600–2500 °C (**b**).

such high temperature as 2500 °C. Thus, the origin of the feature around 287 eV due to hydrogen content can be questionable. Other idea explaining the additional residual feature is that it can be due to the presence of curved fullerene-like bond configuration. Nyberg et al. [63] found that C-K absorption spectra of C_{60} and C_{70} fullerenes consist of double-peaked π^* component. The shoulder on the high energy side of the 1s to π^* peak centered at 287 eV was also confirmed in spectra of fullerenes by other researches [57, 60]. Bearing in mind the results from HRTEM and Raman spectroscopy which indicate that the structure of glassy carbon at different stages of pyrolysis has features of fullerene-like units, we suggest that the EELS spectra of glassy carbons can resemble the spectra of fullerenes. Therefore, we used the ratio of the integrated intensity upon the 287 eV peak ($I_{\pi*np}$) to the area under both 285 and 287 eV peaks ($I_{\pi*total}$) related with the 1s to π^* signal, as a measure of the sp^2 non-planar bond content (sp^2_{np}) to the total (fullerene-like non-planar and graphitic-like planar) sp^2 carbon bonds content (sp^2_{total}), according to the following formula:

$$\frac{sp^2_{np}}{sp^2_{total}} = \frac{I_{\pi*np}}{I_{\pi*total}} \tag{5}$$

This intensity ratio should reflect the degree of curvature of glassy carbon structure due to non-planar, strained sp^2 bonds. The results are presented in Fig. 5b. The dispersion of such determined non-planar sp^2 bond fractions does not exceed 13% of the mean values.

According to the obtained results, the ratio of non-planar sp^2-bonded to all sp^2-bonded carbon atoms increases from approximately 25% for GC600 up to about 38% for GC980 and then a subsequent drop of this ratio is observed to about 30% for GC2500. The

initial increase in the fraction of fullerene-like non-planar sp^2 bonds seems to be a consequence of coalescence of carbon domains. Under the increasing temperature, disordered layers within the glassy carbon merge and connect in various ways, as can be seen in the HRTEM images displayed in Fig. 1. The creation of the postulated non-hexagonal rings during the structure reorganization with heat treatment would explain the revealed rise to the non-planar, strained sp^2 bond content associated with the buckled units. With further increase in the heat treatment temperature, however, more and more defects could be healed progressively providing layers with higher fraction of planar graphitic-like sp^2 bonds.

Mechanical properties and their correlations with the structure

A schematic comparison of the force–displacement response of the studied glassy carbons upon indentation with 800 μN terminal force is shown in Fig. 6. For the sample carbonized at the lowest temperature,
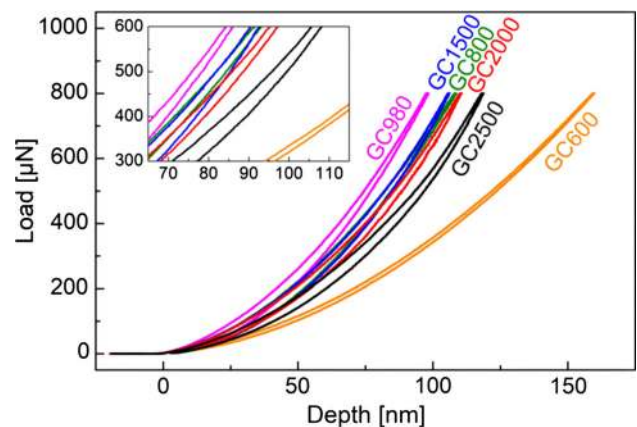
Figure 6 Indentation hysteresis curves of the glassy carbons pyrolyzed at different temperatures from the range of 600–2500 °C (GC600–GC2500).

GC600, the penetration by the indentation is the deepest. A progressive increase in the slope of the load–displacement curve and decrease in the penetration depth are observed up to carbonization at 980 °C. Interestingly, with further increase in carbonization temperature from 980 up to 2500 °C, the material response is reverse and the penetration depth increases gradually. Similar behavior in the temperature range from 1000 to 3000 °C was previously reported by Iwashita et al. [64, 69]. This can be simply explained taking into account the previously described structural changes with increasing pyrolysis temperature. Easier penetration of glassy carbon by indenter can be due to softening of the material during development of more graphitic structure and growth of pores with elevation of heat treatment temperature above around 1000 °C. The unloading paths do not completely retrace the loading paths but return to the origin forming hysteresis loops. The area of the hysteresis loop corresponds to the energy loss during the deformation of the sample surface by the indentation. For the low-temperature glassy carbon, GC600, there is only very small difference between loading and unloading curves, what demonstrates nearly perfect elastic deformation. Moreover, any residual indentation impression after complete loading was observed. This means that the position of indentation tip of the impression at the maximum load goes back to the original sample surface level. The energy dissipation is mostly related with the elastic reversible deformation.

Figure 7 shows the effect of pyrolysis temperature on the hardness and the reduced Young's modulus of the glassy carbons. These mechanical properties for each sample were calculated as averaged values over around 24 measurements of material ability to resist deformation after applying local force. Uncertainties estimated as standard deviations were not greater than 4% for H and 3% for E_r. The values of the determined hardness and reduced Young's modulus rise from around 3.1 and 15.6 GPa, respectively, for glassy carbon carbonized at 600 °C up to around 5.9 and 37.6 GPa, respectively, for 980 °C. With further increase in heat treatment temperature, a continuous decrease in H and E_r is observed up to around 4 and 26.6 GPa, respectively, for 2500 °C. Thus, the effect of pyrolysis temperature on mechanical properties of these polyfurfuryl alcohol-derived glassy carbons in the range of 600–2500 °C can be separated into two ranges: until reaching the temperature of 1000 °C and upon reaching the 1000 °C.

Franklin [10] proposed that the great hardness of the non-graphitizing carbons must be attributed to the strong cross-links between neighboring domains, which may be partially destroyed at high temperatures resulting in hardness decrease. The work of Jenkins and Kawamura [65] shed more light on the changes of glassy carbon mechanical properties during carbonization process. They demonstrated that the hardness increases approximately linearly with the decrease in H/C ratio during material decomposition up to 1500 °C, what is followed by, as they suggested, creation of cross-links and intermolecular forces. Further decrease in mechanical performance for higher heat treatment temperatures is related with breaking some of the cross-link bonds during development of more graphitic structures. Similar conclusions were generally given also by other authors in more recent reports [64, 66, 67].

In the present work, we revealed that the changes in hardness and reduced Young's modulus follow the same trend as the changes in the content of non-planar to the total amount of sp^2 carbon bonds with increase in pyrolysis temperature. Comparison of the data from EELS in Fig. 5b with nanoindentation results in Fig. 7a, b shows that the measured

Figure 7 Variation in the glassy carbon nanoindentation hardness (**a**), and reduced Young's modulus **b** as a function of pyrolysis temperature from the range of 600–2500 °C.
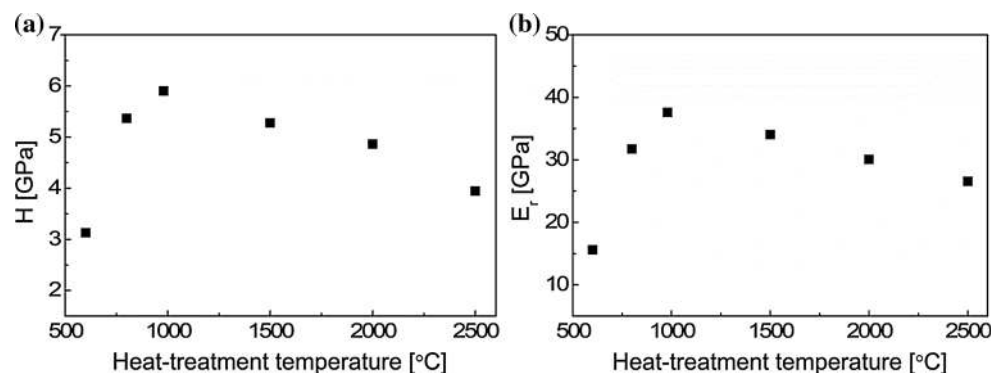
mechanical properties are a direct response of the structural transformation that undergoes with increase in heat treatment temperature. The fraction of sp^2 non-planar, fullerene-like or nanotube-like bonds with respect to the total content of sp^2-hybridized bonds between carbon atoms in structural units can be used for hardness and Young's modulus rating. It is known that carbon nanotubes are one of the strongest materials known [68]. They are also very elastic. It is due to the interlocking carbon-to-carbon covalent bonds. The presence of nanotube-like elements in the structure of glassy carbons can be responsible for their high hardness and strength. The nanotube-like bridges between neighboring carbon layers evident in HRTEM images bind the entire structure into a tight network. It is worth to mention that recently proposed structural models of glassy carbons [60] display the possible configurations of such fullerene-like or nanotube-like interfaces. Based on the models, it was established that the creation of such interlayer connections, or so-called cross-links, is facilitated by the presence of defects in the form of non-hexagonal rings, vacancies, isolated sp^3 bonds or chains which introduce curvature. The curved units may also effectively inhibit the movement of carbon layers and prevent the graphitization.

Conclusions

In this work, the detailed structure studies of the non-graphitizing glassy carbons prepared by pyrolysis of polyfurfuryl alcohol at different temperatures from 600 to 2500 °C and its effect on the mechanical properties of these materials were reported. It was proven that the mechanical properties (hardness and reduced Young's modulus) of the glassy carbons measured via nanoindentation as a function of the pyrolysis temperature are a direct reflection of their internal structure. The presence of fullerene-like or nanotube-like elements in the structure of glassy carbons is considered to be responsible for their high hardness and strength. The hardness and the reduced Young's modulus scale non-monotonically as a function of the pyrolysis temperature reaching maximum values of 5.9 and 37.6 GPa, respectively, for glassy carbon pyrolyzed at 980 °C. The peculiar mechanical behavior of the glassy carbon around 1000 °C is attributed to the greatest amount of non-planar sp^2-hybridized carbon atoms involved in the

building of curved and often interconnected fullerene-like elements at this temperature. The structural curvature seems to be gradually formed at the early stages of the pyrolysis process (at temperatures up to ~ 1000 °C) due to merging of the initial small carbon domains. The cross-links between neighboring graphene-like layers may have nature of non-planar sp^2-type bonds whose content was quantified by EELS measurements. It was demonstrated that at the initial stages of pyrolysis up to 1000 °C the amount of fullerene-like non-planar to total sp^2 carbon bonds increases. Then, with higher heat treatment temperatures the structure is transformed into units composed of greater and less-defected graphite-like domains resulting in decrease in non-planar sp^2 bond content and drop in mechanical performance. In other words, when the material is heated at temperatures higher than 1000 °C, it becomes more ordered but weaker. Therefore, the fraction of sp^2 non-planar fullerene-like or nanotube-like bonds with respect to the total content of sp^2-bonds in the glass-like carbons can be used for evaluation of their mechanical properties.

The knowledge of the structure–property correlations is essential to manufacture glassy carbon products with tailored features. Undoubtedly, one of the most promising glassy carbon's uses is the fabrication of glassy carbon-based super lightweight and strong microlattices. They represent a significant step forward in the field of lightweight mechanical meta-materials and can exert a great impact for medical applications. Due to glassy carbon's good mechanical properties, electrical conductivity, and biocompatibility, this material is interesting for microimplants in the line of microstents, microscaffolds for bone regeneration, and microelectrodes. We hope that the developed here quantitative relationships between the structure and mechanical properties will benefit the further design of the glassy carbon systems.

Acknowledgements

References

[1] Yamada S, Sato H (1962) Some physical properties of glassy carbon. Nature 193:261–262. https://doi.org/10.1038/193261b0

[2] Harris PJF (2004) Fullerene-related structure of commercial glassy carbons. Philos Mag 84:3159–3167. https://doi.org/10.1080/14786430410001720363

[3] Jenkins GM, Kawamura K (1971) Structure of glassy carbon. Nature 231:175–176. https://doi.org/10.1038/231175a0

[4] Jenkins GM, Kawamura K (1976) Polymeric carbons: carbon fibre, glass and char. Cambridge University Press, Cambridge

[5] Driver M (2012) Coatings for biomedical applications. Elsevier, Amsterdam

[6] Harris PJF, Tsang SC (1997) High-resolution electron microscopy studies of non-graphitizing carbons. Philos Mag A 76:667–677. https://doi.org/10.1080/01418619708214028

[7] Harris PJF (1997) Structure of non-graphitising carbons. Int Mater Rev 42:206–218. https://doi.org/10.1179/imr.1997.42.5.206

[8] Harris PJF (2013) Fullerene-like models for microporous carbon. J Mater Sci 48:565–577. https://doi.org/10.1007/s10853-012-6788-1

[9] Harris PJF, Liu Z, Suenaga K (2008) Imaging the atomic structure of activated carbon. J Phys Condens Matter 20:362201–362206. https://doi.org/10.1088/0953-8984/20/36/362201

[10] Franklin RE (1951) Crystallite growth in graphitizing and non-graphitizing carbons. Proc R Soc Lond A Math Phys Eng Sci 209:196–218. https://doi.org/10.1098/rspa.1951.0197

[11] Petkov V, DiFrancesco RG, Billinge SJL, Acharya M, Foley HC (1999) Local structure of nanoporous carbons. Philos Mag B 79:1519–1530. https://doi.org/10.1080/13642819908218319

[12] Jurkiewicz K, Duber S, Burian A (2016) Paracrystalline structure of glass-like carbons. Int J Appl Glass Sci 7:355–363. https://doi.org/10.1111/ijag.12186

[13] Lentz CM, Samuel BA, Foley HC, Haque MA (2011) Synthesis and characterization of glassy carbon nanowires. J Nanomater 2011:129298–129306. https://doi.org/10.1155/2011/129298

[14] Li X, Gao H (2016) Mechanical metamaterials: smaller and stronger. Nat Mater 15:373–374. https://doi.org/10.1038/nmat4591

[15] Kassegne S, Vomero M, Gavuglio R, Hirabayashi M, Özyilmaz E, Nguyen S, Rodriguez J, Özyilmaz E, Niekerk P, Khosla A (2015) Electrical impedance, electrochemistry, mechanical stiffness, and hardness tunability in glassy carbon MEMS µECoG electrodes. Microelectron Eng 133:36–44. https://doi.org/10.1016/j.mee.2014.11.013

[16] Vomero M, Castagnola E, Ciarpella F, Maggiolini E, Goshi N, Zucchini E, Carli S, Fadiga L, Kassegne S, Ricci D (2017) Highly stable glassy carbon interfaces for long-term neural stimulation and low-noise recording of brain activity. Sci Rep 7:40332–40346. https://doi.org/10.1038/srep40332

[17] Zhang ZL, Brydson R, Aslam Z, Reddy S, Brown A, Westwood A, Rand (2011) Investigating the structure of non-graphitising carbons using electron energy loss spectroscopy in the transmission electron microscope. Carbon 49:5049–5063. https://doi.org/10.1016/j.carbon.2011.07.023

[18] Zobelli A, Gloter A, Ewels CP, Seifert G, Colliex C (2007) Electron knock-on cross section of carbon and boron nitride nanotubes. Phys Rev B 75:245402–245411. https://doi.org/10.1103/PhysRevB.75.245402

[19] Jinschek JR, Yucelen E, Calderon HA, Freitag B (2011) Quantitative atomic 3-D imaging of single/double sheet graphene structure. Carbon 49:556–562. https://doi.org/10.1016/j.carbon.2010.09.058

[20] Wojdyr M (2010) Open source GPL'd peak profiling program Fityk. J Appl Crystallogr 43:1126–1128. http://www.unipress.waw.pl/fityk

[21] Oliver WC, Pharr GM (1992) An improved technique for determining hardness and elastic modulus using load and displacement sensing indentation experiments. J Mater Res 7:1564–1583. https://doi.org/10.1557/JMR.1992.1564

[22] Burket CL, Rajagopalan R, Marencic AP, Dronvajjala K, Foley HC (2006) Genesis of porosity in polyfurfuryl alcohol derived nanoporous carbon. Carbon 44:2957–2963. https://doi.org/10.1016/j.carbon.2006.05.029

[23] Cortijo A, Vozmediano MA (2007) Effects of topological defects and local curvature on the electronic properties of planar graphene. Nucl Phys B 763:293–308. https://doi.org/10.1016/j.nuclphysb.2006.10.031

[24] Banhart F, Kotakoski J, Krasheninnikov AV (2010) Structural defects in graphene. ACS nano 5:26–41. https://doi.org/10.1021/nn102598m

[25] Acharya M, Strano MS, Mathews JP, Billinge SJ, Petkov V, Subramoney S, Foley HC (1999) Simulation of nanoporous carbons: a chemically constrained structure. Philos Mag B 79:1499–1518. https://doi.org/10.1080/13642819908218318

[26] Guigo N, Mija A, Vincent L, Sbirrazzuoli N (2007) Chemorheological analysis and model-free kinetics of acid catalysed furfuryl alcohol polymerization. Phys Chem Chem Phys 9:5359–5366. https://doi.org/10.1039/B707950H

[27] Tondi G, Pizzi A, Pasch H, Celzard A, Rode K (2008) MALDI-ToF investigation of furanic polymer foams before and after carbonization: aromatic rearrangement and surviving furanic structures. Eur Polym J 44:2938–2943. https://doi.org/10.1016/j.eurpolymj.2008.06.029

[28] Tuinstra F, Koenig JL (1970) Raman spectrum of graphite. J Chem Phys 53:1126–1130. https://doi.org/10.1063/1.1674108

[29] Pimenta MA, Dresselhaus G, Dresselhaus MS, Cancado LG, Jorio A, Saito R (2007) Studying disorder in graphite-based systems by Raman spectroscopy. Phys Chem Chem Phys 9:1276–1290. https://doi.org/10.1039/B613962K

[30] Thomsen C, Reich S (2000) Double resonant Raman scattering in graphite. Phys Rev Lett 85:5214–5217. https://doi.org/10.1103/PhysRevLett.85.5214

[31] Ferrari AC, Robertson J (2000) Interpretation of Raman spectra of disordered and amorphous carbon. Phys Rev B 61:14095–14107. https://doi.org/10.1103/PhysRevB.61.14095

[32] McCulloch DG, Prawer S, Hoffman A (1994) Structural investigation of xenon-ion-beam-irradiated glassy carbon. Phys Rev B 50:5905–5917. https://doi.org/10.1103/PhysRevB.50.5905

[33] Nakamizo M, Kammereck R, Walker PL (1974) Laser Raman studies on carbons. Carbon 12:259–267. https://doi.org/10.1016/0008-6223(74)90068-2

[34] Rhim YR, Zhang D, Fairbrother DH, Wepasnick KA, Livi KJ, Bodnar RJ, Nagle DC (2010) Changes in electrical and microstructural properties of microcrystalline cellulose as function of carbonization temperature. Carbon 48:1012–1024. https://doi.org/10.1016/j.carbon.2009.11.020

[35] Zickler GA, Smarsly B, Gierlinger N, Peterlik H, Paris O (2006) A reconsideration of the relationship between the crystallite size La of carbons determined by X-ray diffraction and Raman spectroscopy. Carbon 44:3239–3246. https://doi.org/10.1016/j.carbon.2006.06.029

[36] Sze SK, Siddique N, Sloan JJ, Escribano R (2001) Raman spectroscopic characterization of carbonaceous aerosols. Atmos Environ 35:561–568. https://doi.org/10.1016/S1352-2310(00)00325-3

[37] Couzi M, Bruneel JL, Talaga D, Bokobza L (2016) A multi wavelength Raman scattering study of defective graphitic carbon materials: the first order Raman spectra revisited.

Carbon 107:388–394. https://doi.org/10.1016/j.carbon.2016.06.017

[38] Fujimori T, Radovic LR, Silva-Tapia AB, Endo M, Kaneko K (2012) Structural importance of Stone–Thrower–Wales defects in rolled and flat graphenes from surface-enhanced Raman scattering. Carbon 50:3274–3279. https://doi.org/10.1016/j.carbon.2011.12.010

[39] Wu G, Dong J (2006) Raman characteristic peaks induced by the topological defects of carbon nanotube intramolecular junctions. Phys Rev B 73:245414–245422. https://doi.org/10.1103/PhysRevB.73.245414

[40] Piscanec S, Lazzeri M, Mauri F, Ferrari AC (2007) Optical phonons of graphene and nanotubes. Eur Phys J ST 148:159–170. https://doi.org/10.1140/epjst/e2007-00236-2

[41] Charlier JC, Eklund P, Zhu J, Ferrari A (2007) Electron and phonon properties of graphene: their relationship with carbon nanotubes. In: Jorio A, Dresselhaus G, Dresselhaus MS (eds) Carbon Nanotubes. Topics in Applied Physics, vol 111. Springer, Berlin, Heidelberg, pp 673–709. doi:10.1007/978-3-540-72865-8_21

[42] Childres I, Jauregui LA, Park W, Cao H, Chen YP (2013) Raman spectroscopy of graphene and related materials. In: Jang JI (ed) New Developments in Photon Materials Research, vol 1. Nova Science Publishers, New York, pp 1–20

[43] Gupta A, Chen G, Joshi P, Tadigadapa S, Eklund PC (2006) Raman scattering from high-frequency phonons in supported n-graphene layer films. Nano Lett 6:2667–2673. https://doi.org/10.1021/nl061420a

[44] Ferrari AC (2007) Raman spectroscopy of graphene and graphite: disorder, electron–phonon coupling, doping and nonadiabatic effects. Solid State Commun 143:47–57. https://doi.org/10.1016/j.ssc.2007.03.052

[45] Dresselhaus MS, Pimenta MA, Eklund PC, Dresselhaus G (2000) Raman scattering in fullerenes and related carbon-based materials. In: Weber WH, Merlin R (eds) Raman scattering in materials science. Springer, Berlin Heidelberg, pp 314–364. 10.1007/978-3-662-04221-2_10

[46] Dresselhaus MS, Dresselhaus G, Saito R, Jorio A (2005) Raman spectroscopy of carbon nanotubes. Phys Rep 409:47–99. https://doi.org/10.1016/j.physrep.2004.10.006

[47] Rao AM, Richter E, Bandow S, Chase B, Eklund PC, Williams KA, Fang S, Subbaswamy KR, Menon M, Thess A et al (1997) Diameter-selective Raman scattering from vibrational modes in carbon nanotubes. Science 275:187–191. https://doi.org/10.1126/science.275.5297.187

[48] Dresselhaus MS, Dresselhaus G, Eklund PC (1996) Science of fullerenes and carbon nanotubes: their properties and applications. Academic press, Cambridge

[49] Chase B, Herron N, Holler E (1992) Vibrational spectroscopy of fullerenes (C60 and C70). Temperature dependant studies. J Phys Chem 96:4262–4266. https://doi.org/10.1021/j100190a029

[50] Roy D, Chhowalla M, Wang H, Sano N, Alexandrou I, Clyne TW, Amaratunga GAJ (2003) Characterisation of carbon nano-onions using Raman spectroscopy. Chem Phys Lett 373:52–56. https://doi.org/10.1016/S0009-2614(03)00523-2

[51] Tan P, Dimovski S, Gogotsi Y (2004) Raman scattering of non–planar graphite: arched edges, polyhedral crystals, whiskers and cones. Philos Trans R Soc A 362:2289–2310. https://doi.org/10.1098/rsta.2004.1442

[52] Krishnan A, Dujardin E, Treacy MMJ, Hugdahl J, Lynum S, Ebbesen TW (1997) Graphitic cones and the nucleation of curved carbon surfaces. Nature 388:451–454. https://doi.org/10.1038/41284

[53] Zhao X, Ando Y, Qin LC, Kataura H, Maniwa Y, Saito R (2002) Radial breathing modes of multiwalled carbon nanotubes. Chem Phys Lett 361:169–174. https://doi.org/10.1016/S0009-2614(02)00955-7

[54] Singh DK, Iyer PK, Giri PK (2012) Distinguishing defect induced intermediate frequency modes from combination modes in the Raman spectrum of single walled carbon nanotubes. J Appl Phys 111:064304–064314. https://doi.org/10.1063/1.3692070

[55] Ergun S, Tiensuu V (1959) Tetrahedral structures in amorphous carbons. Acta Crystallogr 12:1050–1051. https://doi.org/10.1107/S0365110X59002936

[56] Tessonnier JP, Rosenthal D, Hansen TW, Hess C, Schuster ME, Blume R, Girgsdies F, Pfänder N, Timpe O, Su DS et al (2009) Analysis of the structure and chemical properties of some commercial carbon nanostructures. Carbon 47:1779–1798. https://doi.org/10.1016/j.carbon.2009.02.032

[57] Berger SD, McKenzie DR, Martin PJ (1988) EELS analysis of vacuum arc-deposited diamond-like films. Philos Mag Lett 57:285–290. https://doi.org/10.1080/09500838808214715

[58] Urbonaite S, Wachtmeister S, Mirguet C, Coronel E, Zou WY, Csillag S, Svensson G (2007) EELS studies of carbide derived carbons. Carbon 45:2047–2053. https://doi.org/10.1016/j.carbon.2007.05.0222048

[59] Fink J, Müller-Heinzerling T, Pflüger J, Scheerer B, Dischler B, Koidl P, Bubenze A, Sah RE (1984) Investigation of hydrocarbon-plasma-generated carbon films by electron-energy-loss spectroscopy. Phys Rev B 30:4713–4718. https://doi.org/10.1103/PhysRevB.30.4713

[60] Papworth AJ, Kiely CJ, Burden AP, Silva SRP, Amaratunga GAJ (2000) Electron-energy-loss spectroscopy characterization of the sp^2 bonding fraction within carbon thin films. Phys Rev B 62:12628–12631. https://doi.org/10.1103/PhysRevB.62.12628

[61] Jurkiewicz K, Duber S, Fischer HE, Burian A (2017) Modelling of glass-like carbon structure and its experimental verification by neutron and X-ray diffraction. J Appl Crystallogr 50:36–48. https://doi.org/10.1107/S1600576716017660

[62] Daniels H, Brydson R, Rand B, Brown A (2007) Investigating carbonization and graphitization using electron energy loss spectroscopy (EELS) in the transmission electron microscope (TEM). Philos Mag 87:4073–4092. https://doi.org/10.1080/14786430701394041

[63] Nyberg M, Luo Y, Triguero L, Pettersson LG, Ågren H (1999) Core-hole effects in X-ray-absorption spectra of fullerenes. Phys Rev B 60:7956–7960. https://doi.org/10.1103/physrevb.60.7956

[64] Iwashita N, Swain MV, Field JS, Ohta N, Bitoh S (2001) Elasto-plastic deformation of glass-like carbons heat-treated at different temperatures. Carbon 39:1525–1532. https://doi.org/10.1016/S0008-6223(00)00272-4

[65] Kawamura K, Jenkins GM (1972) Mechanical properties of glassy carbon fibres derived from phenolic resin. J Mater Sci 7:1099–1112. https://doi.org/10.1007/BF00550191

[66] Rodrigues MG, Da Cruz NC, Rangel EC, Zimmerman RL, Ila D, Poker DB, Hensley DK (2005) Effects of ion beam on nanoindentation characteristics of glassy polymeric carbon surface. Surf Coat Technol 196:251–256. https://doi.org/10.1016/j.surfcoat.2004.08.094

[67] Stein IY, Constable AJ, Morales-Medina N, Sackier CV, Devoe ME, Vincent HM, Wardle BL (2017) Structure-mechanical property relations of non-graphitizing pyrolytic carbon synthesized at low temperatures. Carbon 117:411–420. https://doi.org/10.1016/j.carbon.2017.03.001

[68] Yu MF, Lourie O, Dyer MJ, Moloni K, Kelly TF, Ruoff RS (2000) Strength and breaking mechanism of multiwalled carbon nanotubes under tensile load. Science 287:637–640. https://doi.org/10.1126/science.287.5453.637

[69] Iwashita N, Field JS, Swain MV (2002) Indentation hysteresis of glassy carbon materials. Philos Mag A 82:1873–1881. https://doi.org/10.1080/01418610208235699